International Journal of Applied Engineering Research ISSN 0973-4562 Volume 10, Number 13 (2015)

Comparitive Study Of Curvelet And Waveatom Transform In The Classification Of Microcalcifications Using Complex Neural Networks

Dr. E. Malar[a], Priya Krishnamurthy[b], Dr. A. Kandaswamy[c]

[a]Department of Electronics and Communication Engineering,
PSG Institute of Technology and Applied Research, Neelambur, Coimbatore, Tamil Nadu-641062, India,
Ph: +91 9843545796, Email: emalarpsg@gmail. com
[b]Department of Biomedical Engineering, PSG College of Technology, Peelamedu, Coimbatore,
Tamil Nadu-641004, Ph: +91 9655716716, Email: peekay. july@gmail. com
[c]Department of Biomedical Engineering, PSG College of Technology, Peelamedu, Coimbatore,
Tamil Nadu-641004, Ph: +919843057434, Email: kandaswamya@yahoo. com

ABSTRACT:
Mammograms provide a useful tool for diagnosing breast cancer. It is very difficult to classify the microcalcifications as benign or malignant directly by the radiologist from the mammogram images. Therefore in this paper a comparative study based on the curvelet and waveatom features extracted from the mammograms and classification using various classifiers such as Naïve Bayes, ELM (Extreme Learning Machine) and complex ELM has been presented which can be used as a CAD (Computer Aided Diagnosis) system for microcalcification detection. The experimental results were obtained by training and testing data with different classifiers and were compared using classification accuracy obtained. From the results, it was found that the complex extreme learning machine was the best classifier for the waveatom features.

INTRODUCTION:
Mammography is an X-ray imaging technique specially designed for screening soft tissues, i. e., breast tissues and provides the first step in identification of breast cancer. Many women across the globe die due to breast cancer which is the second common cancer affecting women after lung cancer. According to American Cancer Society's reports in 2013, about 39, 620 women will die from breast cancer [1]. The number of deaths due to breast cancer can be decreased by early screening and increased awareness as well as improvements in treatments.
Microcalcifications are tiny calcium deposits which are signs of pre-cancerous changes. They are found as clusters which may be scattered over the entire breast or bilaterally over both breasts. Currently, mammograms are the widely used tools for detection of breast cancer and these microcalcifications appear as tiny bright spots in them. There are chances that the radiologist may miss out these signs by conventional analysis because of the poor contrast obtained in mammograms as well as the huge number of cases that they may have to handle which may cause errors. Thus, a computer aided system integrating the knowledge obtained from radiologist and image processing algorithms along with artificial intelligence will give us a better detection rate and accuracy and thus can help out the radiologist for improved diagnosis. From the given microcalcification it is necessary to identify whether they are benign or malignant. So far, there has been a lot of research going on in this topic which has been listed below. In this paper, the proposed algorithm aims to improve the classification accuracy rates compared to the previous works that have been carried out in the same field.

LITERATURE SURVEY:
Elthouky et al classified mammogram images from MIAS database based on curvelet features using Euclidean distance as a classifier which had an accuracy rate of 98. 59% [2]. J. S. Leena Jasmine et al employed non subsampled contourlet transform and artificial neural network for classification of microcalcifications in mammogram images obtained from MIAS database with average classification rate of 83. 9% [3]. Xinshen Zhang et al used a twin support vector machine and other subspace learning methods like PCA, LDA, TSA and GTDA for microcalcification detection and showed an accuracy of 93. 98±1. 23 for the General tensor discriminant analysis with the twin SVMs[4]. Sandeep Palakkal et al removed Poisson noise from images by combining fast discrete curvelet transform and wave atom with multi scale variance stabilising transform[5]. Fang Liu et al proposed image hashing scheme using waveatom since it had significantly sparser expansion and better characteristics of texture feature extraction than other traditional transforms [6]. Issam El-Naqa et al used a Support Vector Machine (SVM) approach for detecting microcalcification in mammograms which is based on the principle of structural risk minimization and sensitivity as high as 94% was achieved [7]. Fatima Eddaoudi and Fakhita Regragui detected microcalcification in mammograms using Haralick features extracted from texture coded images obtained from MIAS database and classified them using SVM classifier with a classification rate of 95. 6% [27]. Eliza Hashemi Aghjekandi detected microcalcificatiom in mammograms using wavelet transforms and statistical measurements involving skewness and kurtosis [8]. Zehira et al performed a comparative study of different transforms and showed that wave atom transformwas more appropriate for finger print image compression [9]. Hamid Soltanian-Zadeh et al presented a comparison of multiwavelet, wavelet, Haralick and shape features to detect microcalcifications in mammograms using a k-nearest neighbour classifier after feature selection using binary and real valued genetic algorithms. The area under the

ROC curve for the best set of features raged from 0. 84-0. 89 and 0. 83-0. 88 while using real valued and binary genetic algorithms respectively which was by the multiwavlet features that outperformed the other three [16]. Sonyang Yu et al detected microcalcifications using a mix of wavelet features and gray level statistical features and classified it using a general regression neural network via sequential forward and sequential backward selection methods and achieved 90% mean true positive detection rate [10]. Nikhil R. Pal et al proposed a multi-stage detection of microcalcification from mammograms obtained from MIAS database that selected features using a multilayer perceptron network and the classification was done based on the calculation of mountain potential for calcified and normal images separately[24]. J. Jiang et al used the genetic algorithm on images obtained from DDSM database and when it was tested fully on all the images (300 mc and 300 normal) whose area under the ROC curve was 0. 987[25]. E. Malar et al proposed a comparison among statistical texture features, Gabor filter based techniques and wavelet features based fast machine algorithm using Extreme Learning Machine (ELM) for the detection of clusters of microcalcification in digital mammograms with classification accuracy as high as 94% for wavelet features [11]. S. Anand et al proposed directionlet transform for sharpening and enhancement of mammograms and then those features were used for detection of microcalcification and spiculated masses in digitized mammograms. The features were represented in terms of enhancement measure and structural similarity [12]. R. Savitha et al have used fast learning CCELM in real valued classification of mammograms as benign or malignant with 100% classification accuracy compared to ELM and SVM classifiers. Further they have also used it in the classification of emitted acoustic signals based on the source of sound and achieved an accuracy of 99. 27% with only 10 neurons [19].

MATERIALS AND METHODOLOGY:

(i) The DDSM Database

The images obtained for analysis are from a standard database such as DDSM (Digital Database for Screening Mammography)[26] which has been maintained by the University of South Florida. It contains approximately 2500 studies which contains two images of the breast, associated patient information along with some image information.

(ii) Methodology

After pre-processing the images with procedures such as label removal, ROIs of size 512 x 512 were obtained and then used for feature extraction. They were appropriately divided into training(94 images for both benign and malignant) and testing sets(94 which were used for training and testing the different classifiers and to hence find out the most efficient among all the classifiers used. The norm and energy were obtained from the features. The waveatom transform was a single level decomposition whereas the curvelet transform resulted in a seven level decomposition. These in turn were used to classify the data as benign and malignant. Given below is an image pre-processing step, i. e, the extraction of an ROI (Region of Interest) which is the base for the next processing steps. The picture shown below illustrates the steps involved in preprocessing. The image below (Fig. 1) is the left mediolateral oblique view obtained from the DDSM database of a sixty eight year with a tissue density factor of 2.

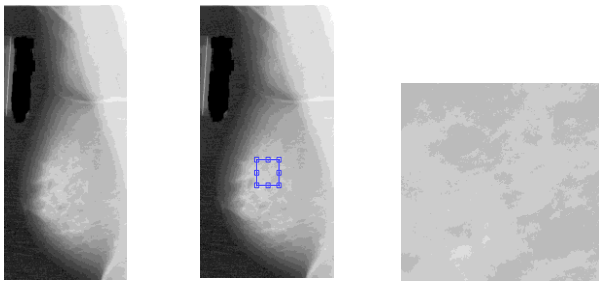

Fig. 1 a) Left MLO view from DDSM database, b) square ROI selector, c) 512x512 ROI

CURVELET TRANSFORM:

A number of research work has been carried out in the area of diagnosing breast cancer with the features extracted from the mammograms using curvelet transform [2, 20]. The description of the curvelet transform implemented via the wrapping algorithm is given below.

The curvelet transform is a multiscale-directional transform through which objects with edges can be given an optimal non-adaptive sparse representation. The curvelet approach requires few coefficients to account for edges and so can easily handle discontinuities. The steps involved for computing curvelet transform are [23]: (1) Subband decomposition, (2) Smooth Partitioning, (3) Renormalization and (4) Ridgelet Analysis.

There are two ways by which curvelet transform can be implemented:

- Curvelets via Unequally Spaced Fast Fourier Transform
- Curvelets via Wrapping

Let *W(r)* and *V(t)* be a pair of windows representing radial window and angular window respectively. These are smooth, nonnegative and real-valued, and W takes positivereal arguments andis supported on r ∈(1/2, 2) and V takes real arguments and is supported on t ∈[−1, 1]. These windows obey admissibility conditions

$$\sum_{j=-\infty}^{\infty} W^2\left(2^j r\right) = 1, r \in \left(\frac{3}{4}, \frac{3}{2}\right) \quad (1)$$

$$\sum_{l=-\infty}^{\infty} V^2(t-l) = 1, r \in \left(-\frac{1}{2}, \frac{1}{2}\right) \quad (2)$$

For each $j \geq j_o$, a frequency window *Uj*defined in the Fourier domain by

$$Uj(r, \theta) = 2^{-j3/4}\, W(2^{-j} r) V\left(\frac{2^{\lfloor j/2 \rfloor}\theta}{2\pi}\right),$$

where $\lfloor j/2 \rfloor$ is an integer part of j/2. The support of *Uj*is a polar wedge defined by the support of W and V, the radial and angular windows. Define the waveform $\varphi_j(x)$ by means of its Fourier transform $\hat{\varphi}_j(\omega) = Uj(\omega)$

$\varphi_j$is the mother curvelet from which all curvelets at scale $2^{-j}$are obtained by rotations and translations of φ_j.

A curvelet coefficient is the inner product between an element$f \in L^2(R^2)$and a curvelet $\varphi_{j,k,l}C(j,\ l,\ k)=\int_{R^2} f(x)\ \overline{\varphi_{j,k,l}(x)}\ dx$, where R is a real line. [2] (3)

In this paper the curvelet transform has been implemented using the wrapping algorithm. The advantages of using this method are that its implementation is a numerical isometry and has effective computational complexity 6 to 10 times than that of an FFT operating on an array of the same size, making it suitable for large scale applications.

The curvelets via wrapping has been described below with basics steps:

Step 1: Compute 2D Fast Fourier Transform (FFT) coefficients to obtain Fourier samples $\hat{f} = [n_1,n_2]$.

Step 2: Interpolation, for each scale and angle pair (j, l), $\widetilde{U_{j,l}}= [n_1,n_2]\tilde{f} = [n_1,n_2]$.

Step 3: Wrap result of step 2 around the origin and obtain $\widetilde{f_{j,l}}= [n_1,n_2]=W(\widetilde{U_{j,l}}\tilde{f})\ [n_1,n_2]$, where the range n_1 and $n_2$are $0 \le n_1 \le L_{1,j}$ and $0 \le n_2 \le L_{2,j}$

Step 4: Implement the inverse 2D FFT to each $\widetilde{f_{j,l}}$ to obtain the discrete coefficients.

The Fourier frequency plane of each image is split into radial and angular wedges in first two steps, because there is a parabolic relationship between the length and width of the curvelet in Figure. Each generated wedge corresponds to curvelet coefficients at a given scale and angle pair. The data re-index around the origin in step 3. Figure 2a and 2b illustrate original and warped segments around the origin, respectively. Finally, inverse FFT is implemented to get curvelet coefficients in the spatial domain.

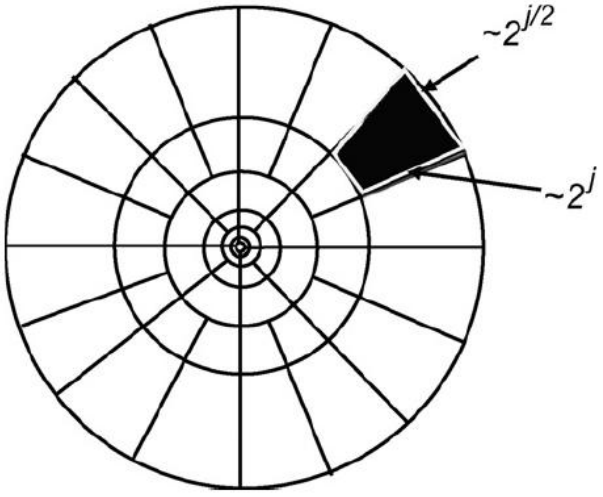

Fig. 2 Curvelet tilting in frequency domain [2]

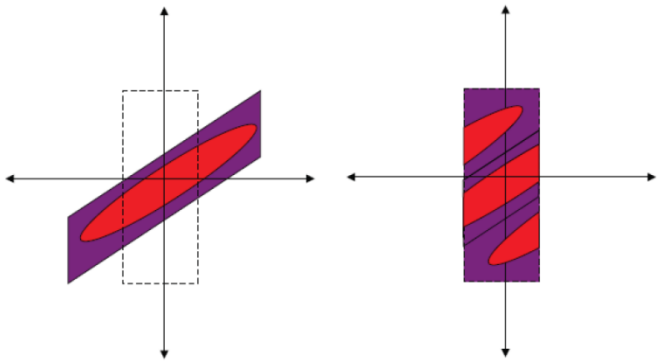

Fig 3a. Original segment. b. Wrapped segment around the origin [20]

In this algorithm, the curvelet transform with seven levels of decomposition has been performed out of which the norm and energy is calculated for the first hundred coefficients after arranging the coefficients in descending order.

WAVE ATOM TRANSFORM

The waveatom transform has been used for applications as suggested in [5, 6, 9, 13, 15]. Therefore, in this paper, this method has been extended by implementing it on mammogram images and further classification as benign or malignant microcalcification using a classifier. The description of the waveatom transform has been given below.

Wave atoms are represented as φ_μ(x), with subscript μ=(j, m, n)=(j, m1, m2, n1, n2). All fivequantities j, m1, m2, n1, n2 are integer-valued and index a point(x_μ, ω_μ)in phase-space, as

$$x_\mu = 2^{-j}\boldsymbol{n},\ \omega_\mu = \pi 2^j \boldsymbol{m}, C_1 2^j \le \max_{i=1,2}|m_i| \le C_2 2^j, \qquad (4)$$

where C1, C2 are two positive constants. Heuristically, *the position vector*x_μ, is the center ofφ_μ(x)and *the wave vector*$\omega_\mu$determines the centers of both bumps of $\varphi\hat{}_\mu(\omega)$ as $\pm\omega_\mu$. Note that the range of m needs to be further reduced to $m_2>0$ (or $m_2=0$ and $m_1>0$) to account for the central symmetry of the Fourier transform of real-valued functions about the origin in ω. Some further restriction on n (cutoff in space) and j (cutoff in scale), are of course necessary in practice, but not for the description of a frame of $L^2(\mathbb{R}^2)$.

Wave atoms then need to obey a localization condition around the phase-space point(x_μ, ω_μ).

The elements of a frame of wave packets$\{\varphi_\mu\}$ are calledwave atoms when

$$|\varphi\hat{}_\mu| \le C_M.2^{-j}(1+2^{-j}|\omega-\omega_\mu|)^{-M}+C_M.2^{-j}(1+2^{-j}|\omega-\omega_\mu|)^{-M} \text{ for all M>0 and}$$

$$|\varphi_\mu| \le C_M.2^j(1+2^j|x-x_\mu|)^{-M} \text{ for all M>0 [13]} \qquad (5)$$

Wave atom transform algorithm is similar to that of curvelet transform with O(N log N) in 1D algorithm and O(N^2 log N) in 2D[14].

Wave atoms take complex values in frequency domain. The name "wave atoms" comes from the property that they also provide an optimally sparse representation of wave propagators with applications to fast numerical solvers for wave equations[15]. Wave atoms yield better asymptomatic rates when compared to curvelets. For wave atoms the wavelength and the diameter are linked by parabolic scaling,
Wavelength~$(\text{Diameter})^2$

Phase-space localization of the wave packets require that

- in x, the essential support of$\varphi_\mu(x)$ is of size $\sim 2^{-\alpha j}$vs. $2^{-\beta j}$ as scale j $\geq$ 0, with oscillations of wavelength $\sim 2^{-j}$transverse to the ridge; and
- in frequency ω, the essential support of $\varphi\,\hat{}_\mu(\omega)$ consists of two bumps, each of size $\sim 2^{\alpha j}$ vs. $2^{\beta j}$ as scale j, at opposing angles and distance $\sim 2^{j}$from the origin.

Two parameters α and β are generally used to describe any wave packet architecture:
α suggests how the scale of decomposition is and β indicates how the waves are directed, i. e., directional selectivity. A value of β=0 means best selectivity and β=1 means poor selectivity. For curvelets α=1 and β=1/2 whereas wave atoms are defined as α=β=1/2 [14].

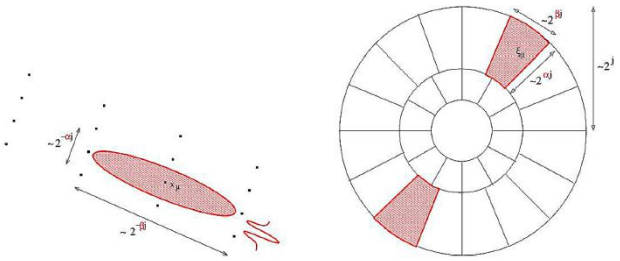

Fig 4. Requirements of a single wave packet defined by the parameters α and β, in space (left) and in frequency (right)

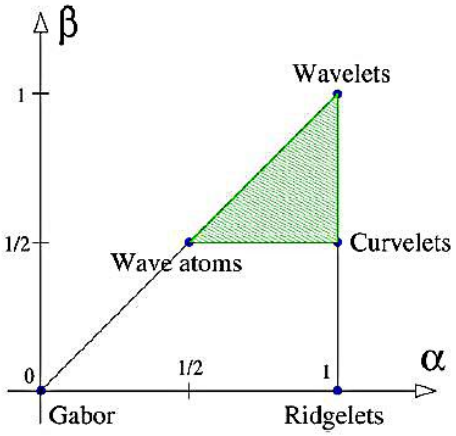

Fig 5. Identification of various transforms as (α, β) families of wave packets.

FLOWCHART:

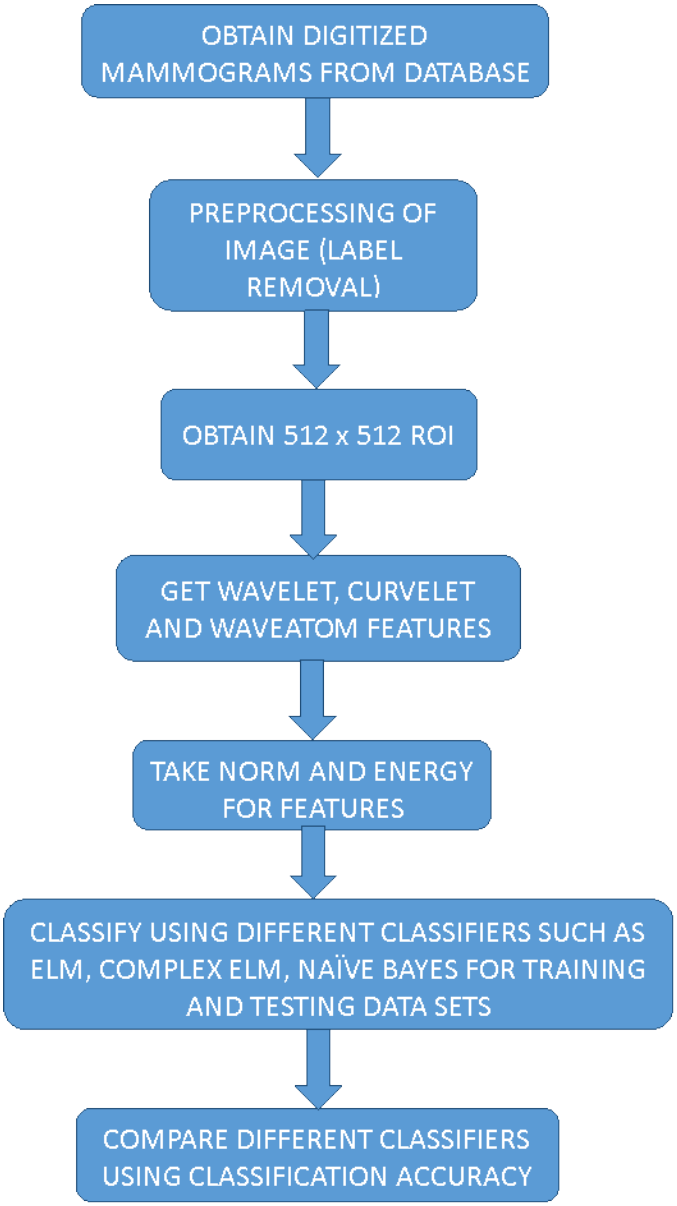

EXTREME LEARNING MACHINE:

The Extreme Learning Machine has been used for various applications like multi-category sparse data classification [18], for classification of mammographic classifications [11], for human face recognition system [21] and for image quality assessment [22].
Here, the ELM classifier has been used for classification of microcalcifications as benign or malignant with the help of features extracted using the curvelet and waveatom transform. These results are then used for comparison with various other classifiers to identify the classifier that gives more accurate classification. Given below is the working mechanism of the ELM classifier.
Extreme Learning Machine is a single layer feed-forward neural network, which follows least square based approach [17] that can randomly choose hidden nodes unlike other classifiers which require to see the training data and the output

weights of the SLFNs are analytically determined. It can not only achieve small training error but also a very small norm of output weights are also obtained. The activation function used in ELM are even discontinuous or nondifferentiable functions [18]. The advantages of using ELM as a classifier are good efficiency, quick learning speed, easy implementation and minimum human intervention. The ELM can obtain the solutions directly without trivial issues such as local minima, improper learning rate and overfitting, etc.

Let $\{X_i, Y_i\}$ be a set of N distinct samples, where $X_i = [x_{i1}, x_{i2}, \ldots, x_{in}] \in \Re^n$ represents the input features and $Y_i = [y_{i1}, y_{i2}, \ldots\ldots, y_{im}] \in \Re^m$ represents its coded class label and with L hidden nodes and activation function *G(x),* the ELM classifier function that assigns class label with desired accuracy can be written as

$$Y=F(X) \tag{6}$$

The output of the ELM function with H hidden neurons is shown below:

$$\hat{Y}=\hat{F}(X_i)=\sum_{l=1}^{H} W_{Okl} G_l(W_i, B_i, X_i), \text{ where } k=1, 2, \ldots, C \tag{7}$$

Where W_O represents the *C* x *H* hidden layer neurons, W_i represents *H* x *n* input layer weights and B_i represents *H* x *1* bias of hidden neurons. $G_l(.)$ represents output of *lth* hidden neuron and *G(.)* is the activation function. If the activation function is sigmoid, it is written as

$$G_l = \sum_{k=1}^{n} G(w_{i\,lk} x_{ik} + b_l) \text{ where } l=1, 2, \ldots, H \tag{8}$$

And for a radial basis function (RBF), the activation function is defined as

$$G_l = \sum_{k=1}^{n} G(\|b_l(X - W_i)\|) \text{ where } l=1, 2, \ldots, H \tag{9}$$

The above equation (7) can be represented in a matrix form as well

$$\hat{Y}=W_O Y_H, \text{ where } Y_H = \begin{bmatrix} G_1(W_i, b_1, X_1) & \cdots & G_1(W_i, b_1, X_N) \\ \vdots & \vdots & \vdots \\ G_H(W_i, b_H, X_1) & \cdots & G_H(W_i, b_H, X_N) \end{bmatrix} \tag{10}$$

and is called hidden layer output matrix of the neural network. By knowing the output $\hat{Y}$, we can estimate the output weights analytically from the formula $W_O = Y Y_H^{\dagger}$, where $Y_H^{\dagger}$ is called Moore-Penrose generalized pseudo-inverse of Y_H.

CIRCULAR COMPLEX ELM:

According to the results in [19], the CCELM classifier has been used for the classification of acoustic signal emission (with five input features) and the classification of breast mass in mammograms as benign or malignant (with nine input features) and the average classification accuracy obtained in both were 99. 17 and 100 percent respectively. Apart from this it was also implemented in problems of image segmentation, vehicle classification and glass identification problems and these results were compared with other classifiers. In this paper, the CCELM classifier has been used for the classification of mammograms as benign or malignant based on the waveatom and curvelet features extracted from the images and a comparison of the classifiers has also been studied.

Due to the presence of inherent orthogonal boundaries, complex valued ELM networks perform better than the real valued networks. It is similar to the normal ELM network that chooses random hidden nodes and calculates the output weights analytically with a difference in activation functions, i. e., circular transformation for input layer, complex function such as 'sech' for hidden layer and linear function for the output layer [19].

The CC-ELM classifier is a single hidden layer network with *m* input neurons, *K* hidden neurons and C output neurons. The circular transformation that transforms the real valued input features to the Complex domain ($\Re \rightarrow \mathbb{C}: \mathbf{x} = [x_1, \ldots, x_m] \rightarrow \mathbf{z} = [z_1, \ldots, z_m]$ is given by

$$z_l = \sin(a x_l + i b x_l + \alpha_l), l = 1, 2 \ldots m \tag{11}$$

Where $a, b, \alpha_l \epsilon \Re^+$ are non-zero constants and x_l is the input normalised feature in [0, 1]. The scaling factors *a*, and *b,* and the translational, rotational bias term α_l are randomly chosen such that $0 < a, b \leq 1$, and $0 < \alpha_l < 2\pi$. These operations make the input features well distributed in the complex plane and hence CC-ELM exploits the orthogonal decision boundaries of the fully complex-valued networks more efficiently.

The neurons in the hidden layer of CC-ELM employ a fully-complex valued 'sech' activation function which is Gaussian like. The response of the *j*th hidden neuron (h_j) is given by

$$h_j = \text{sech}\,[\mathbf{u}_j^T(\mathbf{z} - \mathbf{v}_j)], j=1, 2, \ldots, K \tag{12}$$

where K is the number of hidden neurons, $\mathbf{u}_j \epsilon \mathbb{C}^m$ is the complex-valued scaling factor of the *j*th hidden neuron, $\mathbf{v}_j \epsilon \mathbb{C}^m$ is the complex-valued center of the *j*th hidden neuron and the superscript T represents the matrix transpose operator. The neurons in the output layer employ a linear activation function. The output ($\hat{\mathbf{y}} = [\hat{y}_1 \ldots \hat{y}_n \ldots \hat{y}_c]^T$) of CC-ELM network with K hidden neurons is

$$\hat{y}_n = \sum_{j=1}^{n} w_{nj} h_j, n = 1, 2, \ldots C \tag{13}$$

where w_{ij} is the output weight connecting the *j*th hidden neuron and the *i*th output neuron.

The estimated class label ($\hat{c}$) is obtained using

$$\hat{c} = \arg\max_{n=1,2,\ldots C} real\ part\ of\ \hat{y}_n \tag{14}$$

The output of CCELM classifier in equation (13) is as follows:

$$\hat{Y}= WH \tag{15}$$

where, W is the matrix of all output weights that connect hidden neurons and output neurons. H is the response of hidden neurons for all training samples.

The output weights are estimated by least square methods as:

$$W=YH^{\dagger}, \quad (16)$$

where $H^{\dagger}$ is the generalized Moore-Penrose pseudo-inverse [22] of the hidden layer output matrix and Y is the complexvalued coded class label.

RESULTS AND DISCUSSION:

The mammogram images have been obtained from the DDSM (Digital Database for Screening Mammograms). In this paper a total of 370 images have been used of which 184 images are benign and 186 malignant. From these two categories, the data were split into training (92 for benign and 94 for malignant) and testing sets (92 for both benign and malignant). After the feature extraction using the respective transforms (curvelet and waveatom), the norm and energy from the features were calculated. The distribution of the norm and energy obtained for the curvelet and waveatom features for both the classes have been shown using the box plot.

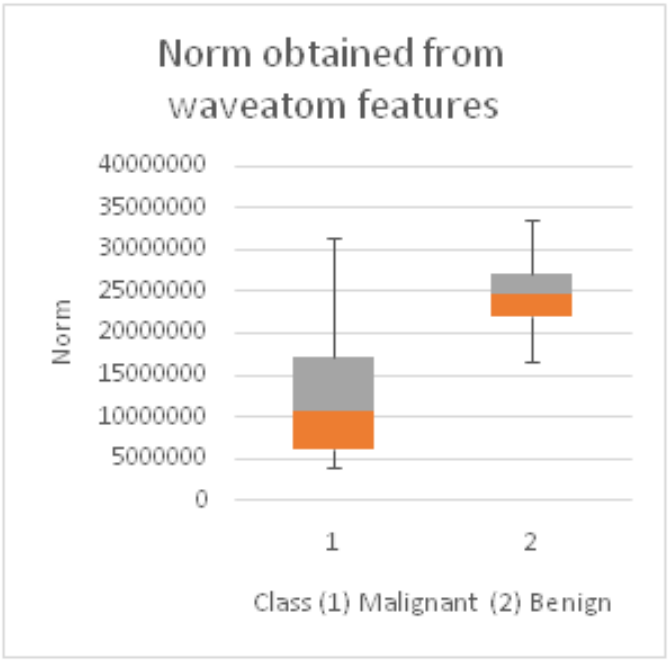

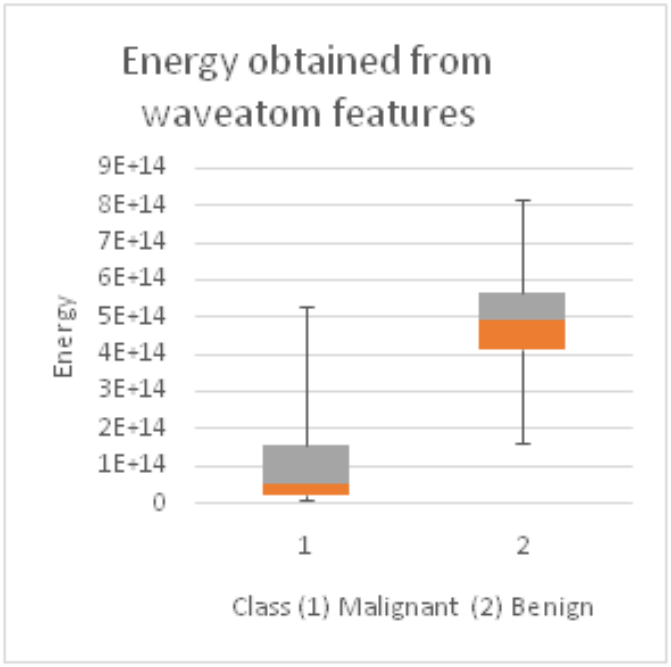

Fig 7. Norm and Energy features obtained from waveatom features showing two different microcalcification classes, i. e., malignant and benign

These features (shown in Fig. 7)obtained show that there is a difference in the values between the benign and malignant images which is identified by the classifier and then used for classification.

The performance of various classifiers such as Naïve Bayes, ELM and CCELM are compared and the results are validated by means of a various parameters such as the classification accuracy, true positive rate, false positive rate, F-measure and precision. They are calculated in the following way:

True Positive Rate (TPR) = $\frac{TP}{P}$

False Positive Rate (FPR) = $\frac{FP}{N}$

Precision (Pr) = $\frac{TP}{TP+FP}$

Accuracy (Ac) = $\frac{TP+TN}{P+N}$

F-measure (F_m) = $\frac{2}{\frac{1}{Pr}+\frac{1}{TPR}}$

The CCELM classifier was tested for different efficiencies by varying the number of hidden neurons and this has been illustrated in fig8. For the waveatom features, the best accuracy is obtained for 20 hidden neurons and for the curvelet features, the best accuracy is obtained for 40 hidden neurons. By increasing the number of hidden neurons, the efficiency drops down.

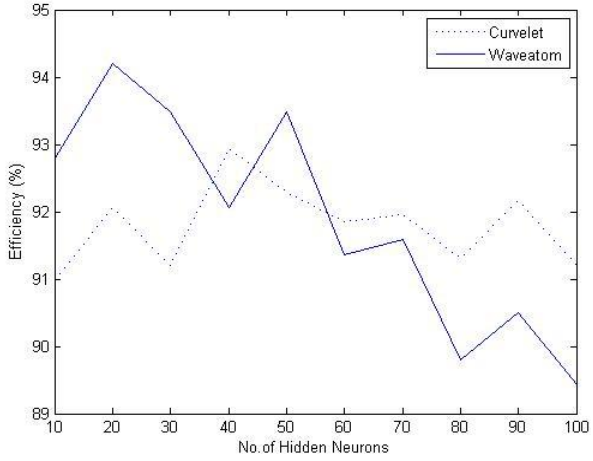

Fig 8. Classification efficiency Vs number of hidden neurons for both curvelet and waveatom features using CCELM classifier

It was found that the CCELM was the best classifier and it showed improved performance with the waveatom features. This result can be validated with the higher values of testing classification accuracy of 93. 5% for the waveatom features compared to 88. 2% with the curvelet features with the CC-ELM classifier. The CC-ELM provides a better classification accuracy than the ELM which provided a result of 90. 76% with the waveatom features. The results are tabulated in the tables below.

Table 1. Results for curvelet features with various classifiers

CURVELET						
					ACCURACY	
CLASSIFIER	TP RATE	FP RATE	F MEASURE	PRECISION	TRAINING	TESTING
Naïve Bayes	0. 859	0. 141	0. 858	0. 861	0. 951	0. 915
ELM	0. 935	0. 076	0. 927	0. 925	0. 989	0. 929
CC-ELM	0. 774	0. 012	0. 931	0. 985	0. 995	0. 882

Table 2. Results for waveatom features with various classifiers

WAVEATOM						
					ACCURACY	
CLASSIFIER	TP RATE	FP RATE	F MEASURE	PRECISION	TRAINING	TESTING
Naïve Bayes	0. 886	0. 114	0. 886	0. 887	0. 971	0. 959
ELM	0. 946	0. 13	0. 893	0. 879	0. 9731	0. 9076
CC-ELM	0. 946	0. 056	0. 94	0. 946	0. 978	0. 935

CONCLUSION:

In this paper, a novel approach has been proposed for using the waveatom transform for applications in medical images in classifying the mammogram classifications as benign or malignant. This has been done by means of using the mammograms obtained from the DDSM database and classifying the microcalcifications using classifiers such as Extreme Learning Machine and the Circular Complex Extreme Learning Machine giving classification accuracy of 90. 76 and 93. 5 respectively. This approach has given us a better result compared to that of the curvelet transform that gives us an accuracy rate of 92. 9 and 88. 2 for the aforementioned classifiers respectively. It can also been inferred that the CCELM classifier gives a constant higher accuracy rate for both the features, i. e. curvelet and waveatom features thus proving to be as one of the best classifiers. This work can be further extended by applying the waveatom transform for other types of cancer detection.

REFERENCES:

[1] www. cancer. org/cancer/breastcancer/detailedguide/breast-cancer-key-statistics. (American Cancer Society)

[2] Mohamed Meselhy Eltoukhy, Ibrahima Faye, Brahim Belhaouari Samir, “Breast cancer diagnosis in digital mammogram using multiscale curvelet transform”, Computerized Medical Imaging and Graphics, 34 (2010), 269-276.

[3] J. S. Leena Jasmine, A. Govardhan, S. Baskaran, “Classification of Microcalcification in Mammograms using Nonsubsampled Contourlet Transform and Neural Network”, European Journal of Scientific Research, Vol. 46 No. 4 (2010), pp. 531-539

[4] Xinsheng Zhanga, Xinbo Gao, “Twin support vector machines and subspace learning methods for microcalcification clusters detection”, Engineering Applications of Artificial Intelligence, 25 (2012), 1062-1072

[5] Sandeep Palakkal, K. M. M. Prabhu, “Poisson image denoising using fast discrete curvelet transform and wave atom”, Signal Processing, 92 (2012), 2002-2017.

[6] Fang Liu, Lee-Ming Cheng, Hon-Yin Leung, Qi-Kai Fu, “Wave atom transform generated strong image hashing scheme”, Optics communications 285 (2012) 5008-5018

[7] Issam El-Naq, Yongyi Yang, Miles N. Wernick, Nikolas P. Galatsanos, and Robert M. Nishikawa, “A Support Vector Machine Approach for Detection of Microcalcifications”, IEEE Transactions On Medical Imaging, Vol. 21, No. 12, December 2002.

[8] Eliza Hashemi Aghjekandi, “Microcalcification Detection in Mammography using Wavelet Transform and Statistical Parameters” (Thesis work-https: //gupea. ub. gu. se/bitstream/2077/28929/1/gupea_2077_28929_1. pdf)

[9] Zehira Haddada, Azeddine Beghdadi, Amina Serir, Anissa Mokraoui, "Wave atoms based compression method for fingerprint images", Pattern Recognition (2013), http: //dx. doi. org/10. 1016/j. patcog. 2013. 02. 004i

[10] Songyang Yu and Ling Guan, "A CAD System for the Automatic Detection of Clustered Microcalcifications in Digitized Mammogram Films", IEEE Transactions on Medical Imaging, Vol. 19, No. 2, February 2000

[11] E. Malar, Dr. A. Kandaswamy, D. Chakravarthy, A. Giri Dharan, "A novel approach for detection and classification of mammographic microcalcifications using wavelet analysis and extreme learning machine", Computers in Biology and Medicine, 42 (2012), 898-905

[12] S. Anand, R. Shantha Selva Kumari, S. Jeeva, T. Thivya, "Directionlet transform based sharpening and enhancement of mammographicX-ray images", Biomedical Signal Processing and Control(2013)

[13] Laurent Demanet, Lexing Ying, "Wave Atoms and Time Upscaling of Wave Equations", Numerische Mathematik, July 2009, Volume 113, Issue 1, pp 1-71

[14] Laurent Demanet, Lexing Ying, "Curvelets and Wave Atoms for Mirror-Extended Images", July 2007, http: //math. mit. edu/icg/papers/mirrorextended. pdf

[15] Laurent Demanet, Lexing Ying, "Wave atoms and sparsity of oscillatory patterns", Applied and Computational Harmonic Analysis, 23 (2007), 368-387

[16] Hamid Soltanian-Zadeh, Farshid Rafiee-Rad, Siamak Pourabdollah-Nejad D, "Comparison of multiwavelet, wavelet, Haralick, and shape features for microcalcification classification in mammograms", Pattern Recognition 37 (2004), 1973-1986

[17] Guang-Bin Huang, Xiaojian Ding, Hongming Zhou, "Optimization method based extreme learning machine for classification", Neurocomputing, 74 (2010), 155-163

[18] S. Suresh a, S. Saraswathi, N. Sundararajan, "Performance enhancement of extreme learning machine for multi-category sparse data classification problems", Engineering Applications of Artificial Intelligence, 23 (2010), 1149-1157

[19] R. Savitha, S. Suresh, N. Sundararajan, "Fast learning Circular Complex-valued Extreme Learning Machine (CC-ELM) for real-valued classification problems", Information Sciences 187 (2012), 277-290

[20] Nebi Gedik, Ayten Atasoy, "A computer aided diagnosis system for breast cancer detection by using curvelet transform", Turkish Journal of Electrical Engineering & Computer Sciences, 2013, 21: 1002-1014

[21] A. A. Mohammed, R. Minhas, Q. M. JonathanWu, M. A. Sid-Ahmed, "Human face recognition based on multidimensional PCA and extreme learning machine", Pattern Recognition, 44 (2011), 2588-2597

[22] S. Suresh, R. Venkatesh Babu, H. J. Kim, "No-reference image quality assessment using modified extreme learning machine classifier", Applied Soft Computing, 9 (2009), 541-552

[23] D. L. Donoho and M. R. Duncan, "Digital Curvelet Transform: Strategy, Implementation and Experiments", Technical Report, Stanford University 1999

[24] Nikhil R. Pal, Brojeshwar Bhowmick, Sanjaya K. Patel, Srimanta Pal, J. Das, "A multi-stage neural network aided system for detection of microcalcifications in digitized mammograms", Neurocomputing, 71 (2008), 2625-2634

[25] J. Jiang, B. Yao, A. M. Wason, "A genetic algorithm design for microcalcification detection and classification in digital mammograms", Computerized Medical Imaging and Graphics, 31 (2007), 49-61

[26] DDSM database: http: //marathon. csee. usf. edu/Mammography/Database. html

[27] Fatima Eddaoudi and Fakhita Regragui, "Microcalcifications Detection in Mammographic Images Using Texture Coding", Applied Mathematical Sciences, Vol. 5, 2011, no. 8, 381-393